

Nudging observed winds in the Arctic to quantify associated sea ice loss from 1979 to 2020

Qinghua Ding,^a Axel Schweiger,^b Ian Baxter^a

a Department of Geography, and Earth Research Institute, University of California, Santa Barbara, Santa Barbara, California 93106

b Polar Science Center, Applied Physics Laboratory, University of Washington, Seattle, Washington 98195

* Corresponding author: Qinghua Ding, qinghua@ucsb.edu

1

Early Online Release: This preliminary version has been accepted for publication in *Journal of Climate*, may be fully cited, and has been assigned DOI 10.1175/JCLI-D-21-0893.1. The final typeset copyedited article will replace the EOR at the above DOI when it is published.

© 2022 American Meteorological Society

ABSTRACT

Over the past decades, Arctic climate has exhibited significant changes characterized by strong Pan-Arctic warming and a large scale wind shift trending toward an anticyclonic anomaly centered over Greenland and the Arctic ocean. Recent work has suggested that this wind change is able to warm the Arctic atmosphere and melt sea ice through dynamical-driven warming, moistening and ice drift effects. However, previous examination of this linkage lacks a capability to fully consider the complex nature of the sea ice response to the wind change. In this study, we perform a more rigorous test of this idea by using a coupled high-resolution modelling framework with observed winds nudged over the Arctic that allows for a comparison of these wind-induced effects with observations and simulated effects forced by anthropogenic forcing. Our nudging simulation can well capture observed variability of atmospheric temperature, sea ice and the radiation balance during the Arctic summer and appears to simulate around 30% of Arctic warming and sea ice melting over the whole period (1979-2020) and more than 50% over the period 2000 to 2012, which is the fastest Arctic warming decade in the satellite era. In particular, in the summer of 2020, a similar wind pattern reemerged to induce the second-lowest sea ice extent since 1979, suggesting that large scale wind changes in the Arctic is essential in shaping Arctic climate on interannual and interdecadal time scales and may be critical to determine Arctic climate variability in the coming decades.

Significance statement

This work conducts a set of new CESM1 nudging simulations to quantify the impact of the observed evolution of large scale high latitude atmospheric winds on Arctic climate variability over the past four decades. Variations in climate parameters, including sea ice, radiation and atmospheric temperatures are well replicated in the model when observed winds are imposed in the Arctic. By investigating simulated sea ice melting processes in the simulation, we illustrate and estimate how large scale winds in the Arctic help melt sea ice in summer. The nudging method has the potential to make Arctic climate attribution more tangible and to unravel the important physical processes underlying recent abrupt climate change in the Arctic.

1. Introduction

The recent warming and sea ice melting in the Arctic have been attributed largely to humaninduced increases in greenhouse gas concentrations (Serreze and Barry 2011; Screen et al. 2021; IPCC 2021). However, global climate models as a group show a more gradual decline in Arctic sea ice (e.g., Kay et al. 2011; Day et al. 2012; Stroeve et al. 2012; Swart et al. 2015; Notz and Stroeve 2016) and more spatially uniform warming in the Arctic atmosphere (Ding et al. 2017, 2019 - hereafter D17, 19; Topel et al. 2019) than observations when the models are forced by anthropogenic forcing. The causes of this discrepancy remain unclear but leading candidates are a) the inability of models to capture important feedback processes to anthropogenic forcing (Liu et al. 2013; Rosenblum and Eisenman 2016; Notz and Stroeve 2016), b) imprecise natural and anthropogenic aerosol forcings applied in models (Fyfe et al. 2021), and c) internal variability that contributed substantially to the observed strong downward trend of sea ice (Winton 2011; Kay et al. 2011; Sigmond and Fyfe 2016; Meehl et al. 2018; Baxter et al. 2019; Huang et al. 2021) in the past decades. An answer to this question has important implications not only for the interpretation of the past Arctic climate change (Deser and Teng 2008; Olonscheck et al. 2019) but also for future projections for the Arctic, such as the question of when we will see the first ice free summer in the Arctic under continued anthropogenic forcing (Wang and Overland 2009; Jahn et al. 2018; Notz and SIMIP Community 2020).

Indeed, recent studies suggest that internal climate variability might be as important as anthropogenic influences on the observed Arctic sea ice decline over the past decades (Kay et al. 2011; D17, 19; Zhang 2016; England et al. 2019; Dong et al. 2019; England et al. 2020). A number of studies collectively suggest that a large part of the observed sea ice decline is linked to low frequency oceanic processes over the past decades that include changes associated with ocean mixing, freshwater storage, the deep ocean circulation, and poleward oceanic heat transport (Zhang 2015; Li et al. 2017; Årthun et al. 2019; Muilwijk et al. 2019; Wang et al. 2019; Polyakov et al. 2020; Dörr et al. 2021). Some internal atmospheric processes are also known to be essential in shaping sea ice variability over the past 40 years. D17&19 show that summertime barotropic high pressure centered over Greenland is a precursor to September sea ice minima on both interannual and interdecadal timescales. The mechanism behind these connections is speculated to operate in a so-called "top-down" scenario, featuring strong subsidence in the boundary layer and related adiabatic warming above sea ice induced by anomalous high pressure situated in the troposphere

(Papritz 2020). This in turn favors enhanced sea ice melt through generating more low-level clouds (Wernli and Papritz 2018; Huang et al. 2021) and increased downwelling long wave radiation (D17,19). D17 uses a series of experiments to examine this hypothesis and finds that this type of circulation variability captures 40% of sea ice decline in September from 1979 to 2015. A different approach, known as a fingerprint analysis focusing on various large ensemble simulations, confirmed that internal variability is important and explains 40 to 50% of observed sea ice decline over the period (D19, Topal et al. 2020). Baxter et al. (2019) further suggests that the same atmospheric process manifested as a circulation trend toward barotropic high pressure over the Arctic is particularly strong in the 6 years from 2007 to 2012. A simultaneous SST cooling anomaly over the tropical Eastern Pacific may play a key role in establishing the high pressure cell over Greenland through generating a Rossby wave train propagating from the lower latitudes toward the Arctic (Baxter et al. 2019; Jeong et al. 2022).

However, experiments in D17 and Baxter et al. (2019) either use a slab sea ice/ocean (no sea ice/ocean dynamics) to couple with an atmospheric general circulation model or prescribe the atmospheric circulation in a complex ice-ocean model. They do not account directly for the feedbacks between the ice-ocean system and the atmosphere. In addition, an internally-favored high pressure pattern in the Arctic detected by the fingerprint analysis in D19 and Topal et al. (2020) or simulated by the tropical SST-imposed experiment in Baxter et al. (2019) still show some differences from the observed counterpart, indicating that the effect of the observed circulation change on sea ice may not be fully replicated in these studies.

Eliminating these limitations in the slab ocean model and developing an integrated, coupled modeling framework in a fully coupled model for a longer period from 1979 to 2020 is necessary to ensure a detailed physical understanding and quantification of the contribution of observed winds to the recent Arctic warming, especially in terms of its importance versus that of external forcing. In particular, following a period of no significant downward trend from 2012 to 2019 (Baxter et al. 2019; Francis and Wu 2020) the sea ice extent of September 2020 reached the second lowest minimum on record. It remains unclear whether the same atmospheric process that contributed to strong melting from 2007 to 2012 reemerged to cause the strong sea ice melting in the summer of 2020 (Liang et al. 2022).

Li et al. (2022) and Roach and Blanchard-Wrigglesworth (2022) recently conducted a number of nudging experiments in CESM1 and find that the wind changes in the Arctic can simulate 25 % of sea ice melting and Arctic upper ocean warming from 1979 to 2018 through the similar atmospheric process identified previously (D17, 19). Using the same approach, Huang et al. (2021) examined summertime interactions between the atmosphere and low level clouds in the Arctic but only focused on the period after 2000 covered by MODIS satellite retrievals. The current study aims to expand these recent efforts by extending the temporal coverage to the period of 1979 to 2020 to better understand the relative contribution of observed wind changes in the recent Arctic warming and sea ice melting. Since Arctic warming and sea ice loss were most rapid during the period from 2000 to 2012 over the past four decades (Baxter et al. 2019), we separately examine circulation variations over this 13-yr period and the whole 42 years to understand how wind changes may have accelerated the sea ice melting over the 13-yr period and how circulation changes from 2000 to 2012 relate to the long term circulation trend over the 42 years. We will also examine the circulation pattern in 2020 to understand a possible forcing of atmospheric processes in contributing to the second lowest sea ice minimum on record.

Many previous analyses have shown that the observed circulation change in the high latitudes of the Northern Hemisphere (NH), manifested as a teleconnection pattern propagating from the tropical Pacific to Arctic (hereafter referred as the Pacific-Arctic teleconnection: PARC), is not well reproduced by the climate model response to global warming. These studies consequently have attributed this circulation change to internal variability originating from the tropics (Ding et al. 2014, D17, D19). Here, we believe that some additional caution should be taken to rethink this assertion since some recent studies have suggested that models' physical biases associated with atmosphere-ocean interactions in the tropics may hinder us from confidently identifying the role of anthropogenic forcing in forming the observed circulation change in the NH (Seager et al. 2019; Wengel et al. 2021). In light of these biases, the main goal of this study is to quantify the contribution of the observed circulation to sea ice loss rather than going further and explore the origin of the observed circulation variability. We believe the presented analysis is a first step toward quantifying the relative roles of internal and external forcing in determining Arctic sea ice changes in future studies.

2. Data and model experiments

a. Reanalysis and sea ice data

We will use monthly ERA5 reanalysis data (Hersbach et al. 2020) and ERSST5 (Huang et al. 2017) from 1979 to 2020 to understand the circulation, temperature, radiation changes and SST over the past 42 years. 6-hourly zonal and meridional winds from ERA5 are used as "observations" to constrain the nudging experiments (see section 2.b). Radiation fluxes at the top of the atmosphere (TOA) and surface are derived from Energy Balanced and Filled (EBAF, Loeb et al. 2018) during the period of 2000 to 2020 to compare with CESM simulations considering that EBAF is constructed by the NASA CERES team using MODIS cloud properties, CERES observed broadband TOA flux measurements, reanalysis meteorological data and assimilated aerosols in calculations with the Fu-Liou radiative transfer model. EBAF is considered a leading benchmarking tool for evaluating the Arctic radiative budget in modelling simulations (Boeke and Taylor 2016; Christensen et al. 2016; Huang et al. 2017).

Observed sea ice monthly data is derived from the National Snow and Ice Data Center (NSIDC) Climate Data Record of Passive Microwave sea ice concentration (SIC), version 3 of the NSIDC (Meier et al. 2017). Given that the most significant change of Arctic sea ice has occurred at the end of the melting season, we focus on total Arctic sea ice area (SIA) for September from observations and model simulations. SIA is calculated as the product of ice concentration and grid element area where ice concentration is greater than 15% and by summing over the entire Arctic region.

b. CESM's forced and nudging experiments

To assess the response of atmosphere and sea ice to anthropogenic forcing over the past decades, we will use 40 realizations of CESM1 large ensembles (CESM-LENS) with small initialization differences for each run (Kay et al. 2014). For our study period 1979-2020 we use CESM-LENS output forced by CMIP5 historical forcing (Taylor et al. 2012) until 2005 and RCP8.5 forcing for 2006-2020. We consider the ensemble mean of CESM-LENS to represent the anthropogenically forced evolution of the climate over the study periods. CESM1 is known to perform reasonably well in simulating many important features of Arctic climate parameters, including annual cycle

of Arctic sea ice extent and spatial distribution of sea ice thickness in the late 20th century (Swart et al. 2015; Labe et al. 2018; England et al. 2019; Notz & SIMIP Community 2020).

Since CESM1, including the atmosphere (CAM5), ocean (POP2), sea ice (CICE4) and land (CLM4.5) component, is the underlying modeling framework for CESM-LENS, for consistency of the comparison, we will use the same version of the fully coupled model (CESM1) to conduct nudging experiments to explore and quantify the influence of the circulation change on sea ice. Nudging experiments (Blanchard-Wrigglesworth and Ding 2019) are a way to "replay" the observed evolution of variability in a coupled model by constraining part of the model domain or selected variables to observations, while others are allowed to vary freely. This approach allows for a direct comparison with observations and the ability to ask "what if" questions and can track sources of variability. In contrast, normal global climate simulations make their own weather and wind changes and can only be compared to observations with respect to statistics over longer time periods. To assess the role of the atmospheric circulation on sea ice trends, our nudging experiments nudge the model's zonal and meridional winds to observations in the Arctic's atmosphere (north of 60°N) from the surface to the TOA. Huang et al. (2021) and Roach and Blanchard-Wrigglesworth (2022) used a very similar approach but nudged the winds above 850hPa in their experiments. A comparison of our results with theirs (not shown) indicates that the sea ice response in CESM1 is not very sensitive to how we set up this nudging in the boundary layer. A buffer zone with a 2 to 3 degrees wide is set on the margin of the nudging domain to allow a smoother transition from full nudging within the domain to no-nudging outside.

The nudging procedure constrains simulated winds within the nudging domain to observed values at the corresponding time, by adding an additional tendency term in the momentum equations at every time step of 30 minutes. 6-hourly reanalysis observations are interpolated to model time steps (30 minutes) by linear interpolation. The magnitude of this tendency term is determined by a weighting parameter varying from zero (no nudging) to one (full nudging). In our experiments, this weighting parameter is selected as one (full nudging) over the entirety of each simulation to force zonal and meridional winds to vary exactly as observed in the model within the Arctic. By doing so, the model will "replay" the observed circulation variability in the Arctic's atmosphere while allowing for responses of other local systems and global climate to the specified wind changes in the Arctic.

The main goal of these nudging experiments is to examine sea ice responses to observed circulation changes over the past decades without direct impacts from anthropogenic radiative forcing. We use winds as a key constraint variable to represent atmospheric circulation variability (Ding et al. 2014; D17). To exclude variability directly related to external forcings (greenhouse gases, aerosols, solar) from nudging experiments, we set external forcings as constant values at the level of the year 2000, which roughly represent the climatological mean values over the 42 years period. In addition, a long spin-up run is needed beforehand to ensure that the nudging simulation has no significant "numerical shock" in the early period when reanalysis winds are imposed in the Arctic since reanalysis winds in the Arctic may be very different from the model's own winds there. To do so, a 150-yr anthropogenic forcing-fixed (at the level of the year 2000) nudging simulation is initially conducted with the model perpetually nudged to winds of year 1979 in the Arctic (the same nudging domain and buffer zone as those used afterwards). In this spin-up, many key indicators of climate stability, including Arctic sea ice, and Pan-Arctic and global mean net radiation at the TOA and surface, start to stabilize after the first 100 years and then vary around constant levels in the last 50 years (Supplementary Fig. 1). At this stage, we believe that the model has taken a sufficiently long time to fully adapt to a new nudging environment in the Arctic and thus any possible numerical drifts due to imposing observed winds are minimized. The model states on Jan 1 of each of the last 10 years of this spin-up are then separately used as initial conditions to reinitiate a set of new 10 members of 42-yr nudging simulations with winds in the Arctic nudged to observations from 1979 to 2020. We then focus on the ensemble mean of the 10 members which represents the influence of winds on sea ice and other fields in the Arctic. We also note that Arctic climate variables simulated by the individual members in the nudging simulations show a relatively small spread away from the ensemble means, likely because a large source of the spread, atmospheric variability, is constrained in these simulations.

3. Simulated Arctic warming due to anthropogenic forcing

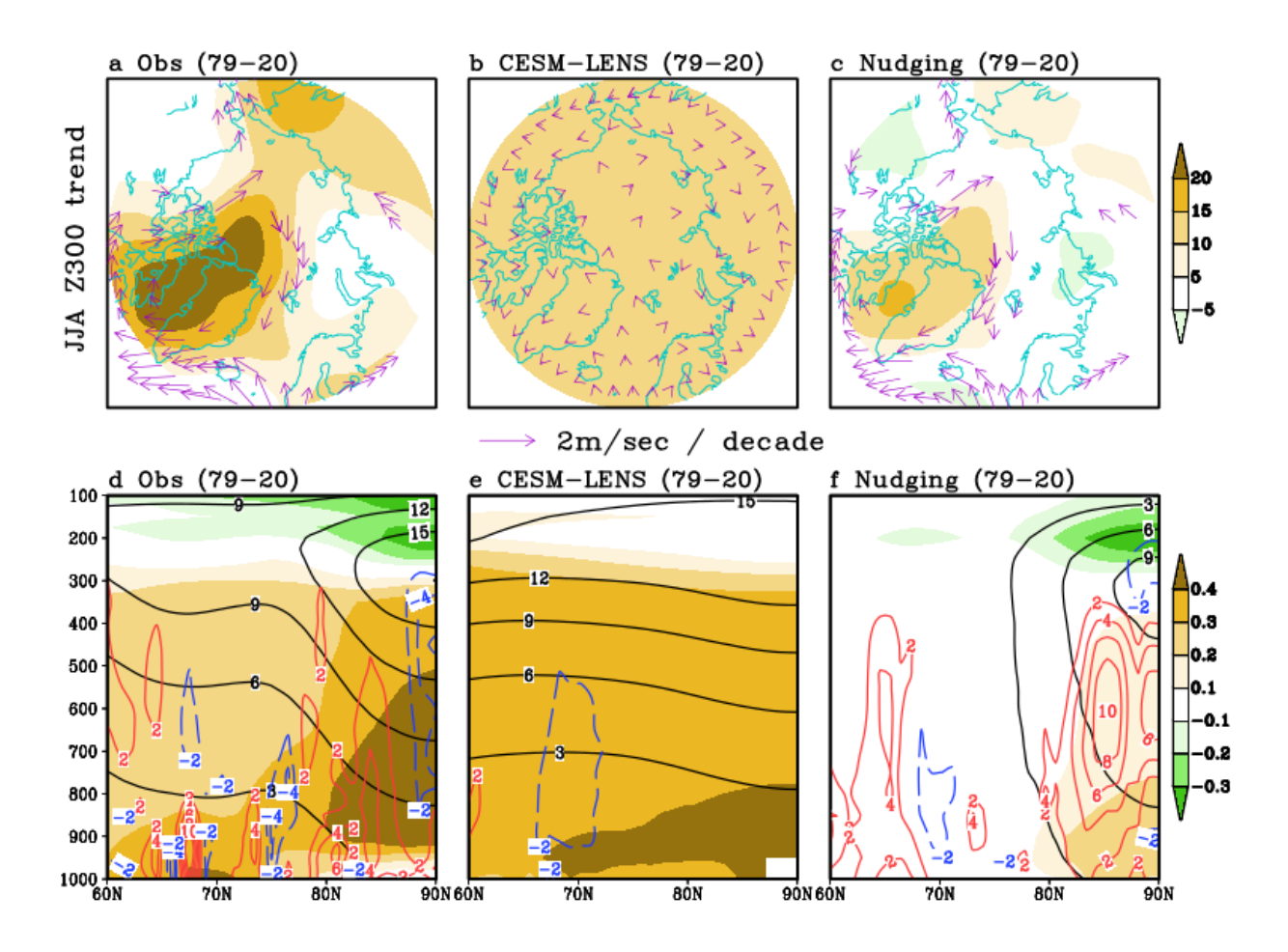


Fig.1 Linear trends of JJA Z300 (shading, m/decade) and winds at 300hPa (vectors, m/s/decade) (a-c, upper panels) and zonal mean geopotential height (black contour, m/decade), temperature (shading, C*/decade) and vertical motion (omega, red (downward motion) and blue (upward motion) contours, 10⁴ Pa/s/decade), (d-f, lower panels) derived from 42 years (1979-2020) (a&d) ERA5, (b&e) the ensemble mean of 40 members of CESM-LENS and (c &f) the ensemble mean of 10-member nudging runs.

Observed Arctic warming in the past four decades (Fig. 1) features a strong anticyclone-like circulation trend in summer that increases greatly over the early 2000s (Fig. 2). From 2000 to 2012, the high pressure is shifted from Greenland toward the interior of the Arctic with 300 hPa winds increased at 10m /decade there. Correspondingly, September sea ice is reduced substantially along the Russian Arctic seas from 1979 to 2020 with an accelerating trend from 2000 to 2012 (Fig. 3). Vertical-latitude transects (60°N -90°N) of zonal mean averages of atmospheric variables (Fig. 1 and 2), show most warming and moistening (not shown) at low levels, with trends around 0.3-0.4 °C/decade from 1979 to 2020 and 1 to 2 °C/decade from 2000 to 2012. This lower tropospheric warming is accompanied by a significant height increase aloft (above 300 hPa) and strong sinking

motion along 80°N. This is a typical circulation configuration during droughts and heat waves at mid and high latitudes (Zschenderlein et al., 2019; Papritz 2020). The surface-friction induced low level divergent winds cause subsidence in the lower troposphere that increase air temperatures and the capacity to hold more moisture. This type of configuration is hereafter referred to as a "top-down" effect of upper level circulation on temperature fields in the lower troposphere.

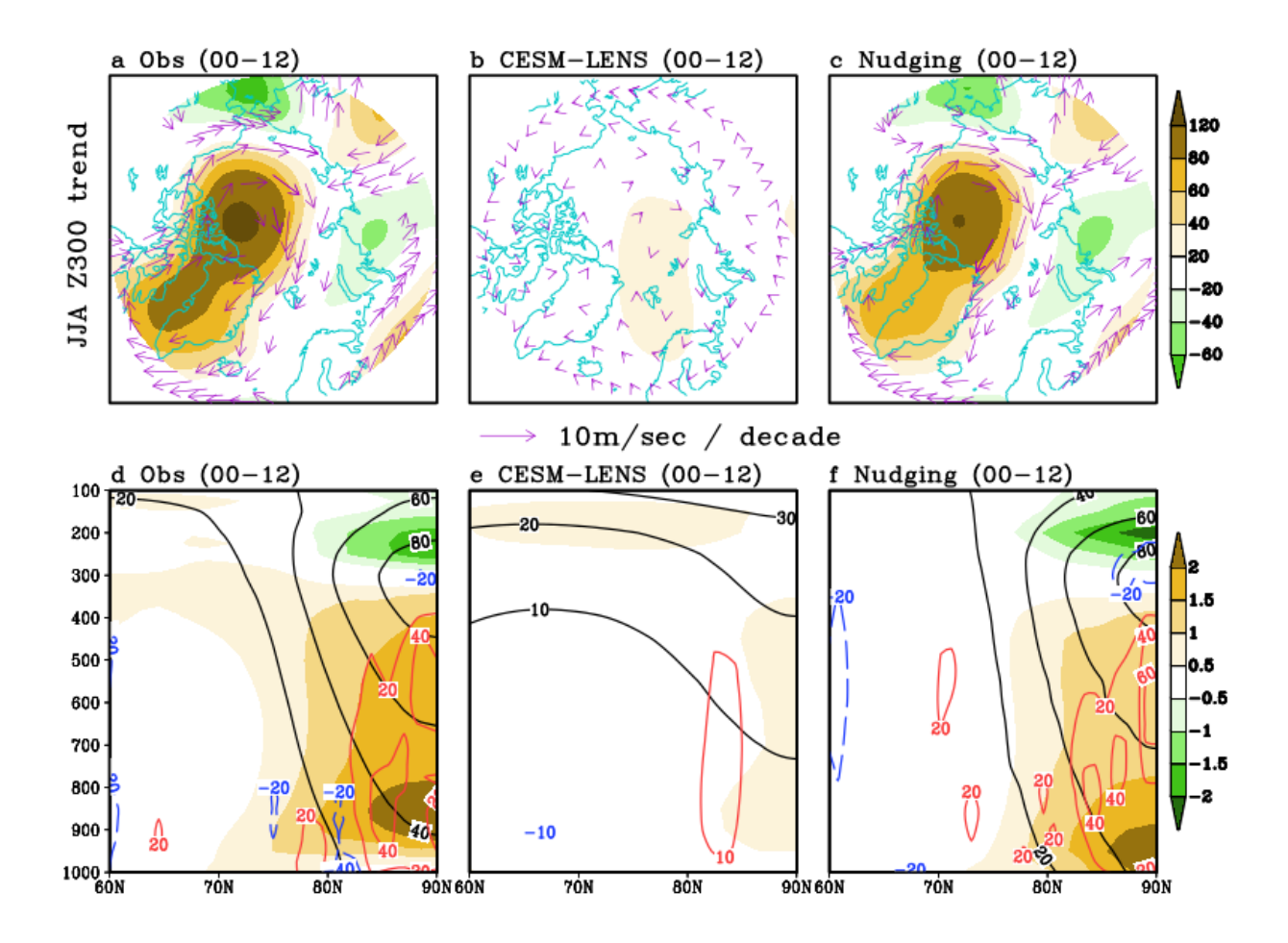


Fig.2 Linear trends of JJA Z300 (shading, m/decade) and winds at 300hPa (vectors, m/s/decade) (a-c, upper panels) and zonal mean geopotential height (black contour, m/decade), temperature (shading, C°/decade) and vertical motion (omega, red contour, 10⁴ Pa/s/decade), (d-f, lower panels) derived from 13 years (2000-2012) (a&d) ERA5, (b&e) the ensemble mean of 40 members of CESM LENS and (c &f) the ensemble mean of 10-member nudging runs.

In contrast to observations, the CESM-LENS ensemble mean, representative of primarily anthropogenic forcing, shows a rather uniform rise of height almost everywhere in the Arctic and

no change in the large scale wind pattern (Fig. 1 and 2). The uniform Z300 height increase due to anthropogenic forcing over and around Greenland only accounts for about 50-60% of the observed changes over the four decades and only 10-20% over the 13 years of the strongest decline. Nevertheless, the sea ice response under anthropogenic forcing shows reductions in ice concentrations in the same places where the observed decline occurs but with weaker magnitude in both 42- and 13-year periods (Fig. 3). In the vertical profile (Fig. 1b and 2b), the troposphere is uniformly warmed in the middle troposphere but the warming is weaker than observed in the lower troposphere over the 13 years. The forced response in the CESM1 favors very weak vertical motion and the induced subsidence trend in the interior of the Arctic only is about 10% of observed changes from 1979 to 2020, and only 20% from 2000 to 2012. This suggests that the direct local impact of external radiative forcing due to increased anthropogenic forcing is quite uniform under the first order approximation and thus cannot drive strong regional pressure gradients, which is the key factor that regulates wind changes and vertical motion. It is still possible that anthropogenic forcing may indirectly generate strong circulation changes in the Arctic via regulating tropical SST variability and tropical SST related teleconnections propagating into the Arctic. However, current models have a limitation reproducing the observed PARC, preventing us from properly examining this possibility (Topal et al. 2020).

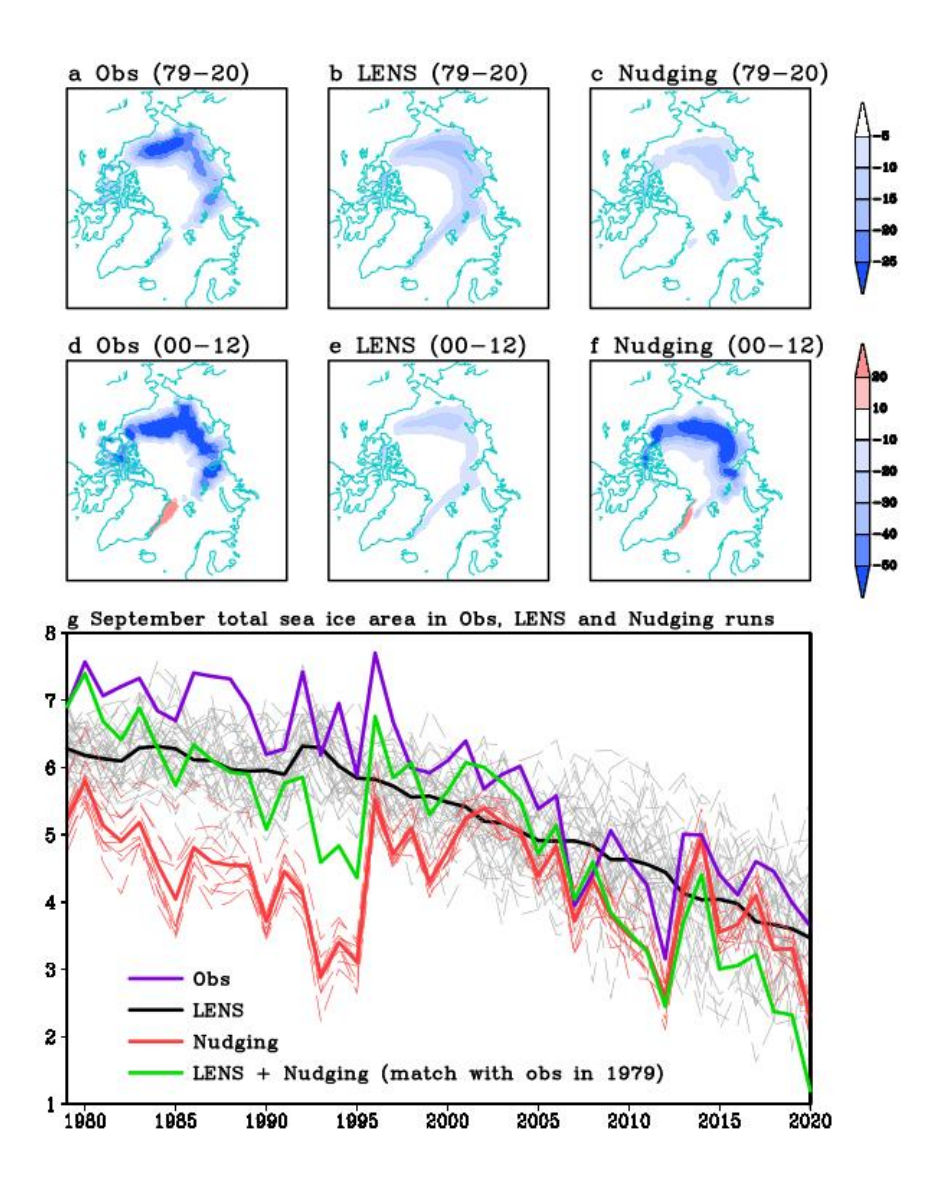


Fig. 3 (upper panels) 42-yr (1979-2020) and (middle panels) 13-yr (2000-2012) linear trends of September sea ice fraction (percent/decade) derived from the (a&d) NSIDC, (b&e) ensemble mean of 40 members of CESM-LENS and (c&f) ensemble mean of 10-member nudging runs. g) The September total sea ice area indices (million km²) constructed based on NSIDC measurement (purple), the ensemble means of each group of simulations (solid, black: CESM-LENS; red: nudging, green: CESM-LENS+ nudging, which is calculated as the arithmetic sum of the time series derived from CESM-LENS and the nudging run, separately. In order to facilitate a comparison with observations, the LENS+nudging starting value in 1979 is adjusted to match with NSIDC data) and individual realizations from each group (dashed line, gray: CESM-LENS, red: nudging).

In the response of these models to anthropogenic forcing, sea ice decline and Arctic warming do exist, but their changing rates are only a portion of observed values for the 42-year period. In particular, over the period from 2000 to 2012 that exhibits the fastest Arctic warming and September sea ice declining trends (-2.2 million km² /decade, Baxter et al. 2019), anthropogenic

forcing alone (-0.8 million square km² / decade) shows a weaker declining trend than observed. The above discussion reaffirms previous results (D17, 19) that the observed circulation changes in the Arctic, that have not been fully explained by current models' responses to anthropogenic forcing, may partially contribute to sea ice loss. What then are the mechanisms by which the atmospheric circulation changes modulate sea ice loss? We adopt our nudging experiments to reveal the mechanisms and quantify how observed large scale circulation changes exert an impact on sea ice.

4. Impacts of large scale winds on Arctic warming

We first examine whether our nudging simulations more closely replicate the observed warming features in the past decades. This will tell us to what degree the large scale circulation, represented by its wind field has been responsible for the observed changes in sea ice. All key variables show a stronger resemblance with observations from 2000 to 2012. In the vertical profile (Fig. 2), bottom heavy warming and moistening (not shown) can be reproduced with the vertical motion generated around the same places as observed, supporting that the "top-down" effect of the large scale circulation pattern, featuring a trend toward a high pressure anomaly in the Arctic, on temperature fields requires a build-up of strong sinking motion close to the surface. In particular, this subsidence is only partially captured in the ensemble means of CESM-LENS from 2000 to 2012, suggesting the necessity of large scale winds in creating a strong sinking motion in the simulation (Fig. 2f). Sea ice loss due to wind changes is also simulated over the Pacific Arctic close to Russia (Fig. 3). The magnitude of decline rates over the Pacific sector is stronger than that forced by anthropogenic forcing in the 13-year period and it alone simulates ~60% of the observed declining rate there in September. A match of the Z300 trend and zonal mean vertical profiles of geopotential height trends is also noted over the 42-year period (Fig. 1), however the circulation driven lower tropospheric warming and sea ice melting from 1979 to 2020 are about ~30% of observed changes (Fig. 3), which is close to that estimated by Roach and Blanchard-Wrigglesworth (2022).

To quantify how wind changes impact the temporal variability of Pan-Arctic sea ice, we compare total September SIA from our nudging simulations, CESM-LENS and observations. The nudging run shows relatively weak trends over the entire period, but a larger decline after 2000 and is very similar to observations from 2000 to 2012. One interesting feature of wind-induced sea

ice loss is that 2012 and 2020 rank as the two lowest SIA years, but wind effects create a stronger decline in 2020 than 2012, which is at odds with observations. Over the entire period, the combination of the two forcings appears to slightly overestimate (~15%) the observed decline with the observed, anthropogenic forcing and wind induced sea ice trends at about 0.91, 0.7, 0.35 million square km²/decade, respectively (Fig. 3) and this overestimation is more substantial (~30%) for the 13 years when the wind change appears to be 90% of observed sea ice decline and anthropogenic forcing simulates 40% of the decline (Fig. 3)

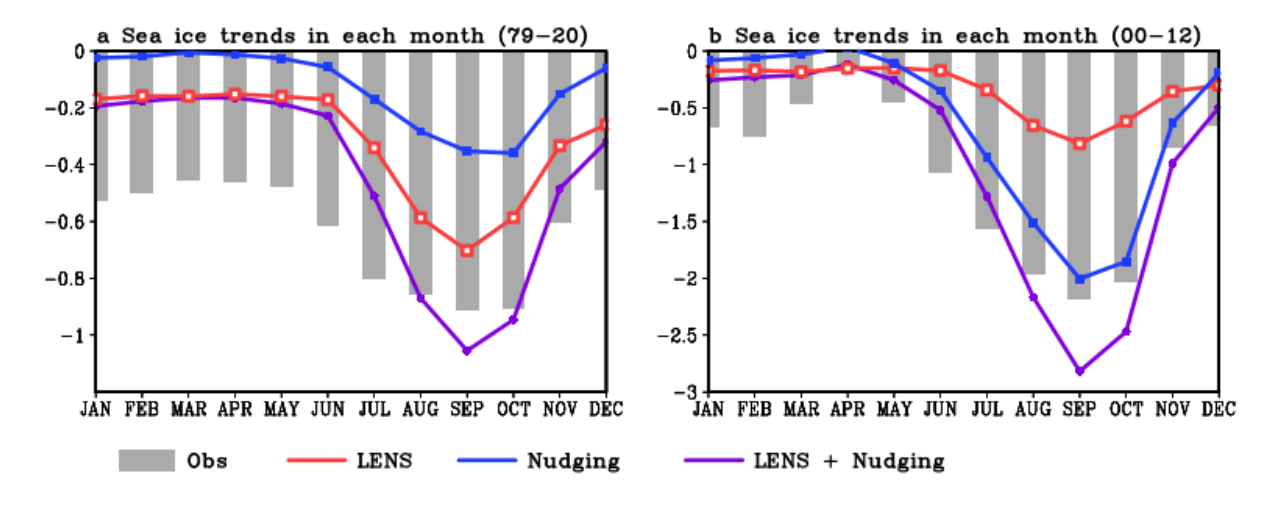


Fig. 4 Linear trends of total sea ice area (million km²/decade) in each month derived from (a) 42 years (1979-2020) and (b) 13 years (2000-2012) of the NSIDC record (gray), the ensemble mean of 40 members of CESM-LENS (red) and the ensemble mean of the 10-member nudging runs (blue). The purple line represents the arithmetic sum of the trends from CESM-LENS and the nudging runs.

We also examine sea ice trends in all months and it is seen that the wind induced sea ice trend capture 40 to 90% of observed changes from June to October from 2000 to 2012 and contributions from anthropogenic forcing are quite stable throughout the year accounting for 30-40% of observed changes (Fig. 4). An overestimation is most prominent from August to October, which is probably due to a possible double-counting discussed in the conclusion section. The combination of the simulated total contribution due to the circulation and anthropogenically-driven contributions to Arctic changes better matches observed changes during the melt season, suggesting that some additional mechanisms that are not well captured in the nudging and forcing runs are also responsible for the melting in the freezing seasons, which requires more attention in future analyses. One possibility is that our nudging domain is only from 60°N to 90°N, which may

not be sufficient to cover all essential wind variability in the high latitudes that are critical to determine wintertime sea ice variability along the periphery of the sea ice edge along 60°N.

Overall, these results show that the observed sea ice change in September over the past 40 years is better simulated by combining anthropogenic and circulation forced changes. This is true regardless of the time period. The correlation of the arithmetic sum of the two SIA time series (the green curve in Fig. 3) with the observed SIA changes (the purple curve in Fig. 3) in September is about 0.81 over 2000-2012 and 0.57 over 1979-2020 for detrended time series (Fig. 3). This suggests that large-scale circulation driven variability not only captures an accelerated decline in sea ice from 2000 to 2012 (Baxter et al. 2019), but also accounts for a large portion of interannual variability. In addition, an early 3-yr sea ice decline forced by the large-scale circulation can be observed from 1992 to 1995, which outpaced the observed decline over the same three years. In contrast, CESM-LENS exhibits a slight increase of sea ice cover over the same period, which is owing to a cooling impact of increased aerosol forcing injected by the Pinatubo eruption into the atmosphere (Lehner et al. 2015; Yang et al. 2019). The arithmetic sum of the trends derived from the two simulations (denoted as CESM-LENS + nudging in Fig. 3) exhibits a better resemblance with the observed changes during these three years. This again suggests that both circulation and external forcing induced sea ice melting should be considered to better understand the observed sea ice variability.

How does the summer atmospheric circulation modulate sea ice decline and help determine September ice extent? The sea ice mass balance is determined by thermodynamic sea ice growth/melt and sea ice dynamics. Sea ice melt can be separated into top, base, and lateral components. We examine the contribution from each process, from June to September in the wind-nudging runs from 2000 to 2012. Top and basal melting from June to September have a strong upward trend from 2000-2012 (Fig. 5) except in peripheral areas where the ice has melted away and leads to a reduction in ice melt. Top melt increases most strongly in July as the warming reduces the albedo due to snow melt and increased ponding etc. (Light et al. 2014; Webster et al. 2018). Lateral melt shows no broad increase except for an area in the Eastern Beaufort, South of Svalbard and along the southern Greenland coast. However, its contribution to the total melting of September sea ice is very trivial compared with basal and top melt within the basin. Sea ice mass transport is plotted to estimate how much of ice is flushed out of the basin due to the wind-drifting

impact (Fig. 5i-l). As a response to large scale circulation changes, characterized by an anticyclonic wind trend pattern, the trend of ice mass transport exhibits a strong anticyclonic tendency from 2000 to 2012 but there is no clear out-of-basin flux through the gateways of the Pacific and Atlantic. To further quantify relative contributions from thermodynamical and dynamical processes to sea ice melting in summer, the trend of the change rate of sea ice volume resulting from each process and their combined effect in JJAS is calculated. The negative (positive) values in Fig. 6 means that the melting (growth) rate due to a particular process is accelerated over the period. It is clear that over the 13 years, most of sea ice volume loss in (about 97%) JJAS is due to thermodynamic processes within the basin and only 3% is due to dynamic/transport processes, suggesting that the summer sea ice decline in the nudging runs is mainly due to wind induced thermodynamical processes within the basin, rather than wind-driven dynamical effects. We also examine the same melting processes simulated in the ensemble means of CESM-LENS. Over the same time period, CESM1 forced by anthropogenic forcing only yields a half of the values captured by the nudging runs, indicating a more direct role of large scale atmospheric circulation in melting sea ice over the period (Supplementary Fig. 2 and 3).

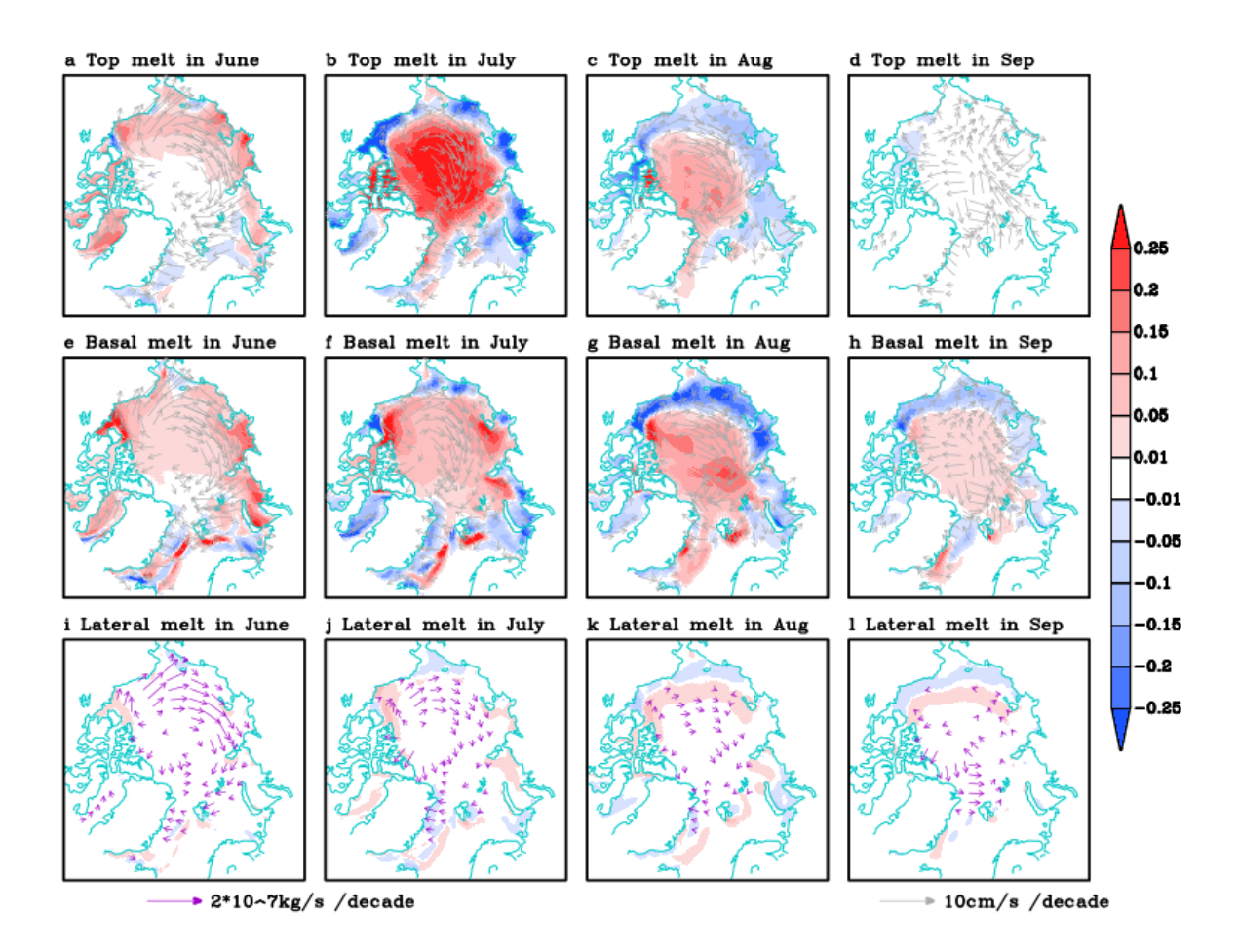


Fig. 5 Linear trends of different type melting processes (shading, m/month/decade), sea ice advection (upper and middle panels, gray vectors) and ice mass transport (lower panels, purple vectors) from June to September derived from 13 years (2000-2012) 10-member mean of nudging runs.

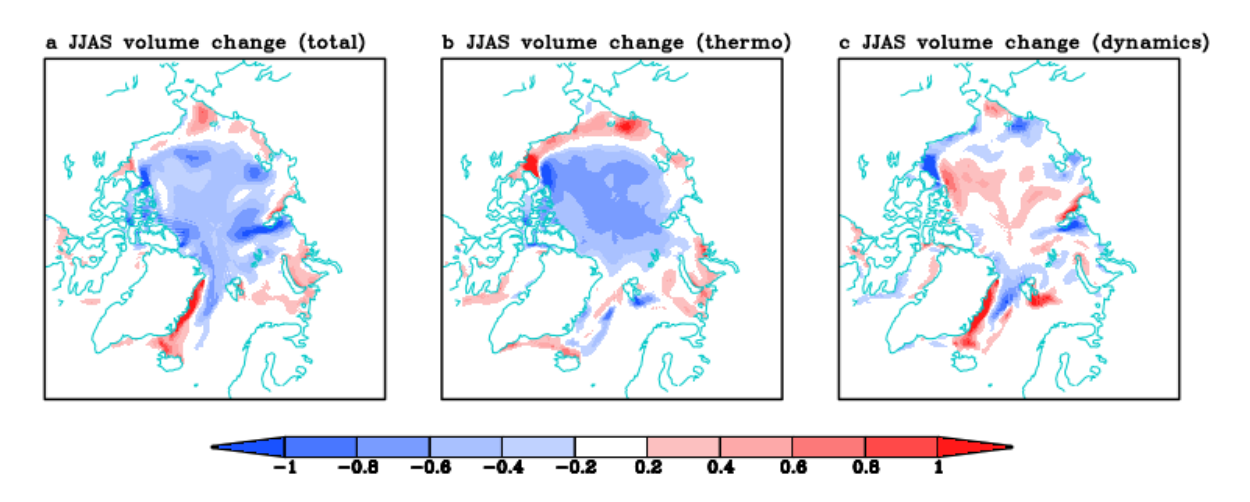


Fig. 6 Linear trends of volume change during JJAS due to a) a combined effect of thermodynamcis and dynamics and b) &c) their respective contribtuions (m/decade) derived from 13 years (2000-2012) 10-member mean of the nudging runs. The Pan Arctic mean in b is -0.25m/decade while the mean in c is -0.01m/decade.

5. Importance of large scale winds in shaping the energy budget in the Arctic

Many of the surface heat and budget terms involved in sea ice changes are difficult to directly validate with direct observations. However, this is different at the TOA where satellite measurements provide multi-decadal records of the energy balance. A comparison of energy budgets at the TOA provides an indirect assessment whether nudging experiments constrained by reanalysis winds provide a realistic simulation of the energy fluxes at the TOA. Since TOA fluxes depend on the correct representation of both vertical and horizontal processes between the surface and the TOA, agreement between model simulations and measurements provides additional confidence that system energetics are accurately reflected in the simulation. We therefore compare the simulated energy budget with EBAF satellite derived measurements. While radiation in ERA5 is primarily model based, it covers an extended record over EBAF which is limited to 2000-2020 and thus can provide an approximate calculation of radiation variability over the entire 42-year period.

The observed change of the JJA net flux at the TOA in ERA5 (Fig. 7) exhibits a slight increasing trend (1.9 W/m²/decade) over the past 42 years, resulting from a cancellation of a strong increase of net downward shortwave radiation (SW) (2.3W/m²/decade) and increased outgoing longwave radiation (LW) (-0.4W/m²/decade). However, the model reflecting primarily anthropogenic forcing (CESM-LENS ensemble mean) shows a trend of (4.4W/m²/decade) which is two times larger than the ERA5 trend. The nudging run does much better to replicate the energy budget (1.6W/m²/decade) on both interannual and long term time scales with numerous prominent fluctuations well captured and the net flux explains 25% (R-square) of the variance in ERA5. From 2000 to 2012, the nudged simulations closely match EBAF with trends of 9.3 W/m²/decade and 10.4 W/m²/decade respectively and capturing 74% (R-square) of the variance in EBAF. This comparison suggests that winds and their impact on the radiatively relevant state of the atmosphere strongly constrain the TOA energy budget. The increase of net SW at the TOA over these 13 years reflects a reduction of the total planetary albedo, which is primarily determined by a reduction of surface albedo when the surface becomes darker with less sea ice coverage in JJA (Fig. 3). This spatial pattern in EBAF is well captured in the nudging run but reflective of the somewhat weaker sea ice loss in the nudging run. The forced simulation driven by anthropogenic forcing simulates

a weak but very uniform increase almost everywhere in the basin since sea ice melting in the forced run is more homogeneous than observations (Fig. 3).

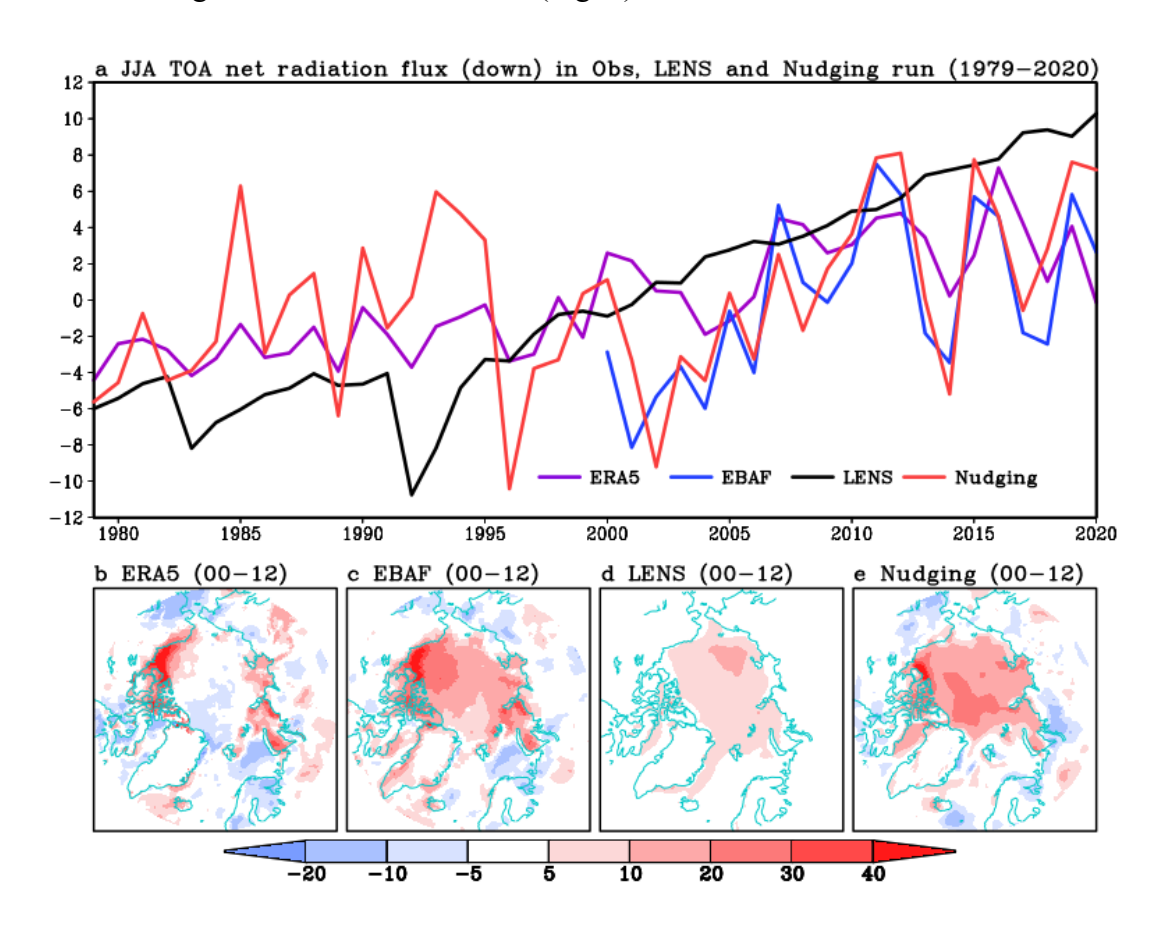


Fig. 7 a) Anomalous JJA net radiation flux (W/m²) at the TOA averaged within the Arctic (70°N -90°N) derived from 42 years (1979-2020) ERA5, the ensemble mean of 40 members of CESM-LENS and the ensemble mean of 10-member nudging runs and 21 years (2000-2020) EBAF. b) to e) Spatial patterns of 13 years (2000-2012) linear trends of JJA net radiation flux (W/m²/decade) at the TOA from each dataset. Positive (downward) value indicates that the atmosphere gains heat.

At the surface (Fig. 8), the net radiation flux change shows a very similar variation as the net flux at the TOA (r_{raw}=0.91 and r_{detrend}=0.73 in ERA5), suggesting that the net radiation change at the TOA is primarily shaped by the net radiation flux at the surface in reanalysis. The net radiation flux change at the surface in ERA5 has an upward trend (into the surface) from 1979 to 2020 (2.7 W/m²/decade) and a stronger trend from 2000 to 2012 (5.6 W/m²/decade in ERA5 and 10.9 W/m²/decade in EBAF), all of which show similar variations as that at the TOA. The CESM-LENS generates a stronger upward trend (4.5 W/m²/decade) than ERA5 over the whole period and its spatial pattern is very different from the observed counterparts in ERA5 and EBAF from 2000

to 2012 (Fig. 8d). The fact that the nudging run (without any increases in anthropogenic forcing) is able to replicate the trend in the TOA and surface energy budget (Fig. 7 and 8), is evidence that over the relatively short period, atmospheric variability dominates TOA and surface radiation fluxes. This increase of net radiation flux at the surface is mainly due to an increase of downward LW and reflected SW (Supplementary Fig. 4 to 7). These changes reflect impacts of a significant ice-albedo feedback and warming air overlying the sea ice (Donohoe et al. 2020). Although the run driven by anthropogenic forcing is able to replicate changes in Arctic wide averages, the spatial pattern of the response exhibits some differences from those observed, featuring rather uniform changes almost everywhere within the Arctic. This suggests that wind induced atmospheric warming may serve as an additional factor along with anthropogenic forcing to trigger the sea ice-albedo feedback through increasing downward LW, leading to sea ice melt, and subsequent decreases in reflected solar radiation. These comparisons strongly suggest that large scale winds are an essential factor constraining the energy budget at the surface and the TOA. With this forcing added, the model is better constrained to replicate observed energy variability on interannual and interdecadal time scales in the Arctic.

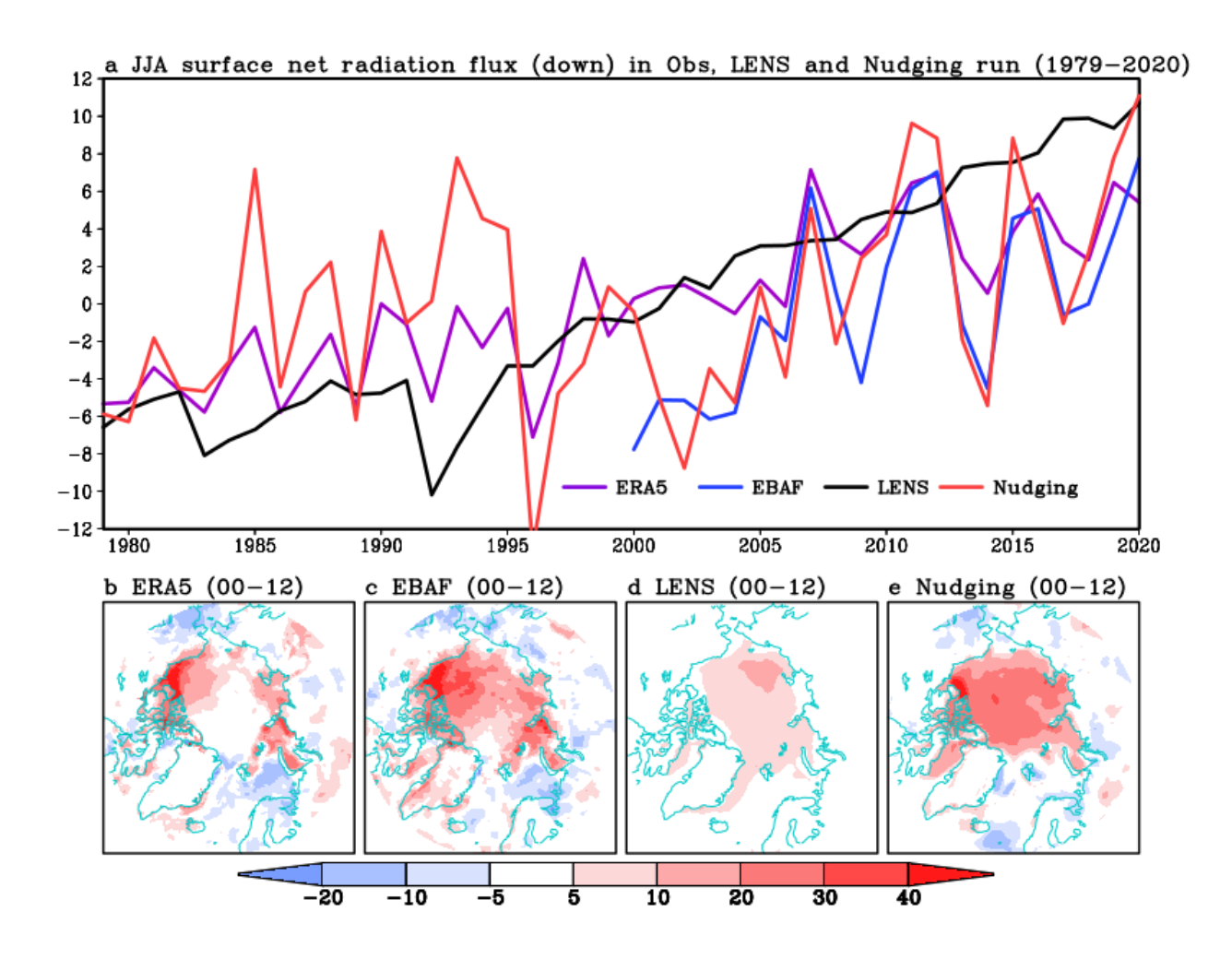


Fig. 8 a) Anomalous JJA net radiation flux (W/m²) at the surface averaged within the Arctic (70°N -90°N) derived from 42 years (1979-2020) ERA5, the ensemble mean of 40 members of CESM-LENS and the ensemble mean of 10-member nudging runs and 21 years (2000-2020) EBAF. b) to e) Spatial patterns of 13 years (2000-2012) linear trends of JJA net radiation flux (W/m²/decade) at the surface from each dataset. Positive (downward) value indicates that the surface gains heat.

6. Circulation pattern in the summer of 2020

Arctic sea ice experienced significant melting in the summer of 2020 which rivals 2012 that still holds the historical record for September sea ice extend minimum. A few studies have attributed the record of 2012 to fit into the tropical-driven teleconnection (e.g., Baxter et al. 2019, Jeong et al. 2022). The near record 2020 September SIA minimum leads us to explore the large scale circulation pattern in the summer of 2020 and ask if it exhibits a similar high pressure anomaly as the trend observed from 2000 to 2012. The magnitude of Z300 within the Arctic (70°N -90°N) ranks as the third highest since 1979 (figure not shown). The vertical structure of geopotential

height, temperature and vertical motion also indicate that the same "top-down" mechanism creates lower-troposphere warming reaching 2-3 °C, which triggers a sea ice-albedo feedback via enhanced dowelling LW (Fig. 9). This similarity with the pattern identified from 2000 to 2012 suggests that atmospheric circulation variability contributed to the near record September sea ice extent in 2020. The nudging run also indicates that the wind induced sea ice melt generates the strongest melt in 2020 over the past 42 years, even 5% stronger than that in 2012, although this difference is likely below the uncertainty of the attribution procedure. Another possibility to explain this difference is that a cooling effect due to some oceanic processes in offsetting atmosphere-induced warming in 2020 (Liang et al. 2022) is not well simulated in our nudging runs. The wind induced JJA atmospheric anomalies in 2020 have very similar vertical structure and magnitude as those derived from ERA5, clearly showing a "top-down" effect manifested by strong downward motions associated with bottom-heavy warming. Simulated sea ice melt in August and September in 2020 also bears strong resemblance to observations with prominent melting over the Russian side of the basin (Fig. 10). In particular, in August, the significant sea ice melting over the region close to north of Greenland and the Canadian Arctic Archipelagos, which is defined as the Last Ice Area (LIA, 81.5°N-85°N, 10°W-50°W), raised awareness within the community about the vulnerability of sea ice over the region where sea ice is previously assumed to be most resilient to global warming (Schweiger et al. 2021). By adding winds, our model simulates similar changes over this region in 2020 and over the 42 years. This suggests that large scale wind variability and its associated thermodynamical and dynamical forcings are critical to determine not only Pan-Arctic changes but also some regional features of sea ice within the basin and nudging simulations can be helpful in understanding the underlying processes in extreme events.

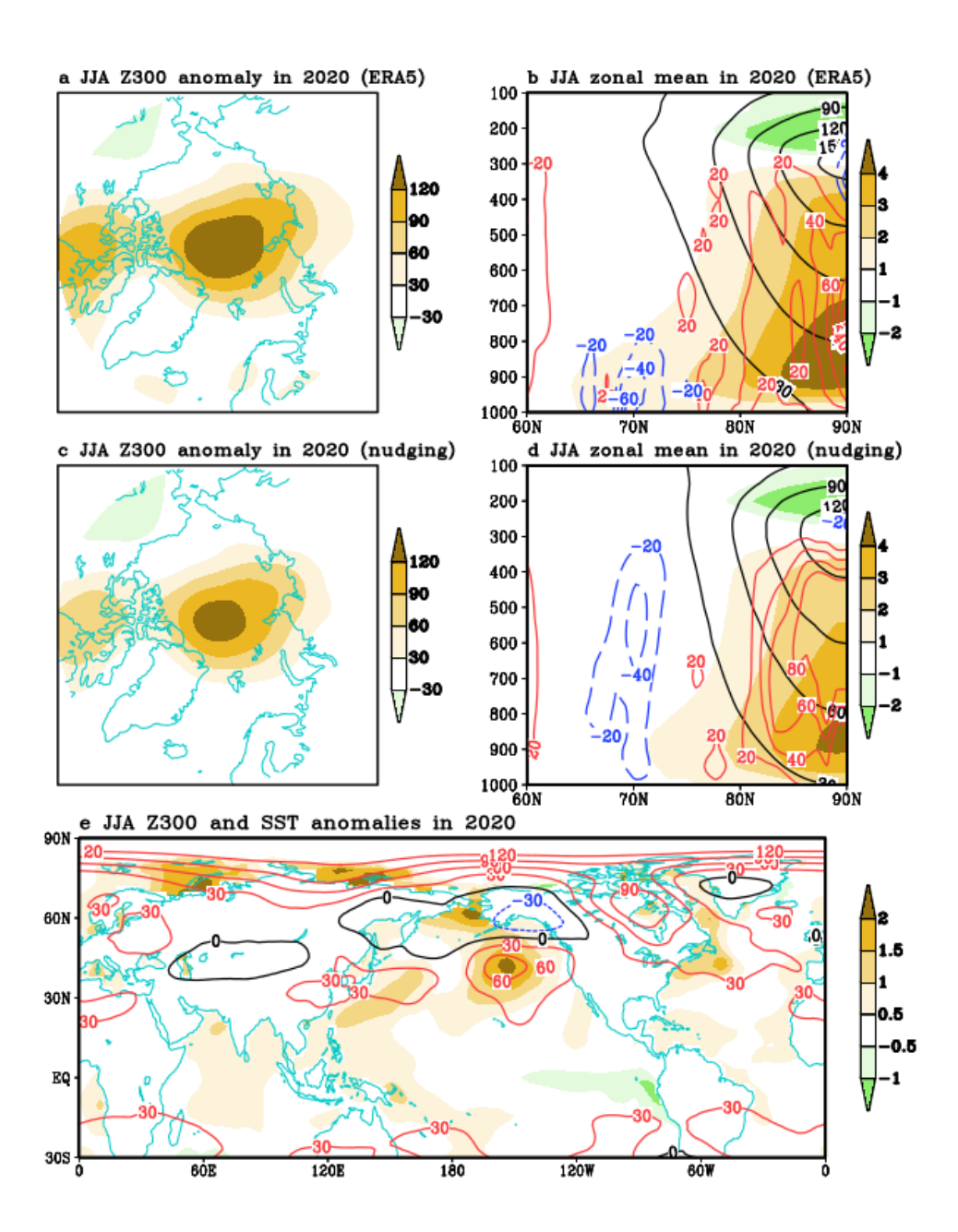


Fig. 9 Anomalous a) and c) Z300 (m) and b) and d) zonal mean geopotential height (black contour, m), temperature (shading, C°) and vertical motion (red contour, 10^4 Pa/s) within the Artic after a removal of the 42-yr (1979-2020) average of corresponding variables in ERA5 and 10-member nudging run. e) Z300 (contour, m) and SST (shading, C°) in the Northern Hemisphere in JJA of 2020 after a removal of the 42-yr (1979-2020) average of corresponding variables in ERA5 and ERSST5.

What is the driver of large scale wind anomalies in the summer of 2020? Baxter et al. (2019) found that the PARC may be responsible for 6-year substantial sea ice melting from 2007 to 2012 driven by SST cooling anomalies in the tropical eastern Pacific with a high pressure anomaly established within the Arctic. In 2020, weak cooling SST anomalies gained strength from May to July and developed into a weak to moderate La Nina by the end of the summer (Fig. 9). Meanwhile, the JJA circulation anomalies over the entire Northern Hemisphere in 2020 are characterized by some features of the PARC teleconnection with two high pressure centers in the Arctic and central North Pacific, respectively and low pressure over Alaska. Thus, JJA high pressure anomalies within the Arctic may have been partially generated by remote tropical cooling in the eastern Pacific. However, a thorough analysis of the tropical origin of JJA Arctic circulation anomalies in 2020 is necessary, which is beyond the scope of this study. In all, the good correspondence between strong sea ice melting and local circulation anomalies in the summer of 2020 gives us more confidence that the high pressure pattern is critical to shape sea ice change not only on low frequency time scales but also in individual years.

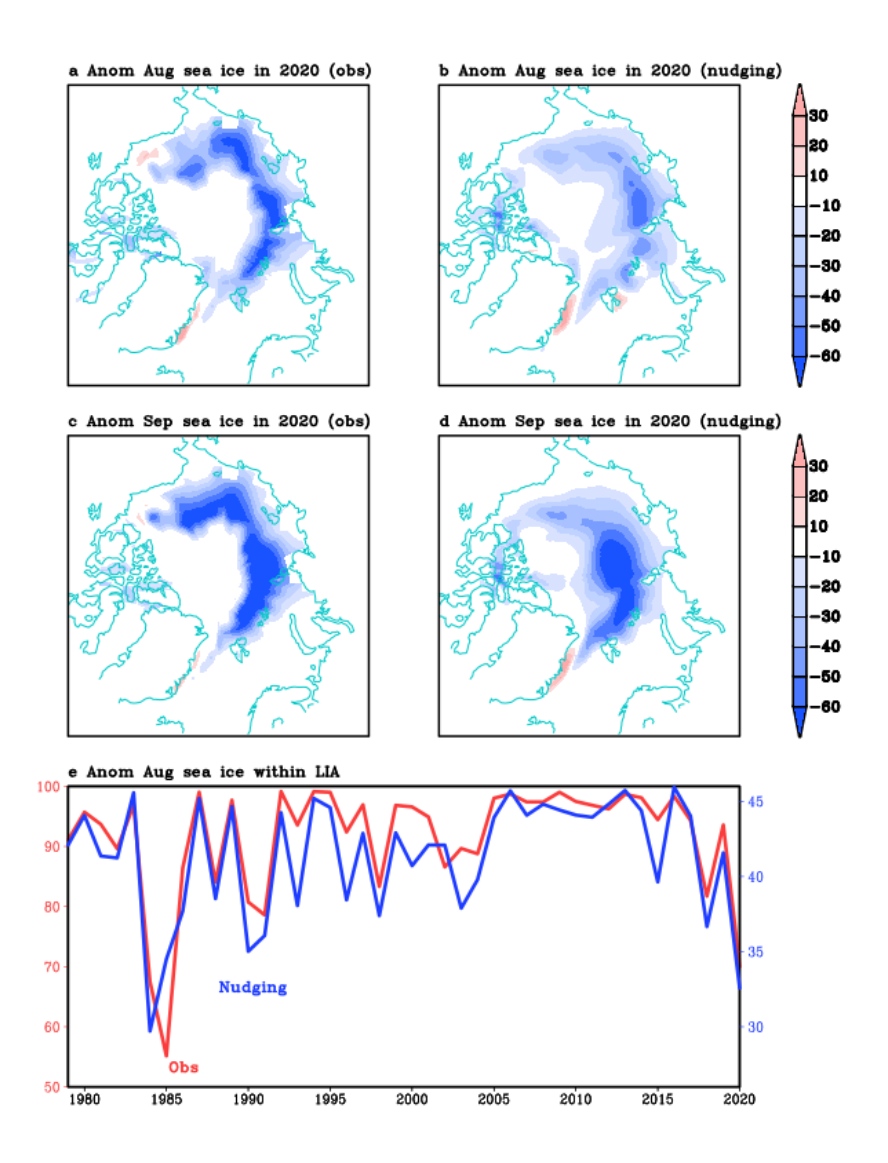


Fig. 10 Anomalous sea ice concentration (Percent) in August and September of 2020 after a removal of the 42-yr (1979-2020) average of corresponding variables in a) and c) NSIDC and b) and d) 10-member nudging run. e) August sea ice concentration (Percent) averaged within the LIA (81.5°N–85°N, 10°W–50°W) from NSIDC and 10-member nudging run during the period 1979 to 2020.

7. Summary and Conclusion

To examine a hypothesis that atmospheric circulation change in the Arctic is a significant contributor to sea ice variability in the past decades, we perform a historical "replay" simulation with the CESM in which zonal and meridional winds in the Arctic atmosphere are fully nudged to the observed fields derived from reanalysis data. The model experiments show that this nudged circulation has a strong control on many key fields in the Arctic that are critical to shape sea ice

variability in summer. By nudging the model's wind field to observations, simulations of temperature, sea ice and radiative fluxes at the TOA and surface are better constrained than those only driven by external anthropogenic forcing on both interannual and interdecadal time scales. Observed sea ice changes appear to be better constrained by a combined impact from high latitude winds and anthropogenic forcing. The melting of sea ice due to wind change is primarily attributed to wind induced adiabatic warming in the Arctic troposphere that in turn triggers ice-albedo feedbacks over sea ice. The melting of sea ice mainly occurs in the basin, of which is primarily basal and top type melting, while the drifting effect due to wind changes may play a minor role in causing lateral melting close to Greenland.

Our attribution based on the wind nudging and historical experiments suggests that from 1979 to 2020 dynamically driven wind change and anthropogenic forcing simulate ~30% and ~70-80% of observed sea ice decline in September, respectively. For the shorter period from 2000-2012 which featured particularly strong melt, our estimate is 50-90% contribution by wind induced changes. However, we should be cautious that this attribution may double count the contribution of winds and still contains large uncertainties. This large uncertainty range and the doublecounting may be due to a number of reasons: 1) the model's sensitivity to winds and anthropogenic forcing may not be exactly the same as that in the real world so we cannot expect that the combined contribution from these two forcings perfectly match with observations. 2) Some wind changes over these periods may be also due to increasing anthropogenic forcing but the CESM-LENS has difficulty in capturing these components so we cannot estimate the significance of this overlapping part. 3) Some other important melting process (e.g., oceanic processes and heat and moisture transport from the lowers latitudes) are not well simulated by the nudging and forced run since these processes may be sensitive to either initial conditions or variability outside our nudging domain (Zhang 2005; Yeager et al. 2015; Polyakov et al. 2020). Thus, future studies are needed to replicate our results using different models so that the uncertainty of our attributions can be evaluated. Although these existing uncertainties hinder us from achieving a very accurate quantification of the relative role of winds and anthropogenic forcing in warming the Arctic over the past decades, it is still very clear that in the same model world, the wind forcing can contribute to a substantial Arctic warming that is comparable with that due to anthropogenic forcing over the whole period and even stronger than that from 2000 to 2012.

Our wind nudging experiment also shows that there is a short wind induced melting period over 1993 to 1995 that is not seen in the observations. The aerosol cooling due to the Pinatubo eruption may exert a cooling forcing to offset this effect, so the observed record reflects a cancellation of a cooling effect of volcanic eruption and a wind induced melting (Lehner et al. 2015; Yang et al. 2019). Over the period 2000- 2012, since both anthropogenic forcing and wind impact favor a strong melting, they cause an accelerated decline in concert from 2000 to 2012. From 2013 to 2019, the wind induced change starts to level off and thus the sea ice decline yields a slowdown tendency, which is mostly attributed to continuously increasing anthropogenic forcing. Thus, wind-induced variability plays a complementary role to either mask or strengthen the impact of external radiative forcing on sea ice depending on the sign of the anomalous circulation pattern prevailing in the Arctic. Thus, this wind change may be an important source of atmospheric variability in the Arctic that complicates our understanding of model responses to anthropogenic forcing. A good example that the enhanced sea ice melting by this atmospheric variability continues to play a role in creating new near record sea ice minima is provided by the summer of 2020, during which a clear high pressure anomaly and its related "top-down" effect on the temperature field are clearly observed in the Arctic.

Although it was suggested that most climate models may have lower sensitivity to anthropogenic forcing in the Arctic than observations (Notz and Stroeve 2016; Rosenblum and Eisenman 2016; Notz and SIMIP Community 2020), here we emphasize that this conclusion may be premature considering that the discrepancy between the forced change and the observed counterpart may not only be determined by models' sensitivity to external radiation forcing. Here we show that observed changes in the Arctic are partially attributable to the response to the large scale atmospheric circulation change. Whether this large scale atmospheric change is entirely due to internal variability of the climate system remains unclear. Several approaches have been proposed to address this issue, which may move us forward to better understand models' sensitivity to internal and external climate forcing (Screen and Deser 2019; Deser et al. 2020). This line of thought focusing on a better evaluation of models' sensitivity has strong implications for future projections of the Arctic climate given that the occurrence of the first ice free summer is subject to strong internal variability. There is some debate about where this internal variability originates (Jahn et al. 2016; Bonan et al. 2021). Some studies have pointed out that the internal source of high latitude circulation is in part generated remotely while others favor local Arctic feedbacks

(Francis and Wu 2020) and oceanic processes (Zhang 2015; Li et al. 2017; Wang et al. 2019; Dörr et al. 2021). While we believe the tropical forcing dominates (Ding et al. 2014; Trenberth et al. 2014; Meehl et al. 2018; McCrystall et al. 2020), at least during summer (D17,19), it is still unclear whether linkages of local circulation with remote forcing is stable (Bonan et al. 2020; Feng et al. 2021) over longer periods and how tropical driven changes in the Arctic will vary on low-frequency time scales in the future (Screen and Deser 2019). In particular, how climate models replicate this remote linkage remains an open question. Thus, a better prediction of high latitude circulation variability in climate models may help to reduce the uncertainty associated with the future projection of Arctic climate in summer.

Acknowledgments.

Predictions This project is supported by Modeling, Analysis, **Projections** and (NA19OAR4310281) and Climate Variability & Predictability (NA18OAR4310424) programs as part of NOAA's Climate Program Office and NSF's Polar Programs (OPP-1744598). A. S. was supported by NSF grants OPP-1744587, PLR-1643436, NASA grant 80NSSC20K1253 and World Wildlife Foundation G-1122-035-00-I. We acknowledge the CESM Large Ensemble Community **Project** and NSF/CISL/Yellowstone supercomputing provided by resources (https://doi.org/10.5065/D6RX99HX) and the CESM Polar Climate Working Group.

Data Availability Statement.

All reanalysis data used in this study were obtained from publicly available sources: ERA5 reanalysis data can be obtained from the ECMWF public datasets web interface (http://apps.ecmwf.int/datasets/). Simulated global circulation, temperature and sea ice under anthropogenic forcing were obtained from the CESM-LENS archives accessed through the Earth System Grid Federation data portal (http://esgf.llnl.gov). In addition, the data generated for this paper and the CESM1 nudging experiment raw output is available from the corresponding author upon request.

References

- Årthun, M., T. Eldevik, and L. H. Smedsrud, 2019: The role of Atlantic heat transport in future Arctic winter sea ice loss. *J. Climate*, **32**, 3327–3341.
- Baxter, I., and Coauthors, 2019: How tropical pacific surface cooling contributed to accelerated sea ice melt from 2007 to 2012 as ice Is thinned by anthropogenic forcing. *J. Climate*, **32**, 8583-8602.
- Blanchard-Wrigglesworth, E, and Q. Ding, 2020: Tropical and midlatitude impact on seasonal polar predictability in the community earth system model. *J. Climate*, **32**, 5997-6014.
- Boeke, R. C., and P. C. Taylor, 2016: Evaluation of the Arctic surface radiation budget in CMIP5 models. *J. Geophys. Res. Atmos.*, **121**, 8525–8548.
- Bonan, D. B., and E. Blanchard-Wrigglesworth, 2020: Nonstationary teleconnection between the Pacific Ocean and Arctic sea ice. *Geophys. Res. Lett.*, 47, e2019GL085666.
- Bonan, D. B., T. Schneider, I. Eisenman, and R. C. J. Wills, 2021: Constraining the date of a seasonally ice-free Arctic using a simple model. *Geophys. Res. Lett.*, **48**, GL094309.
- Christensen, M. W., A. Behrangi, T. S. L'ecuyer, N. B. Wood, M. D. Lebsock, and G. L. Stephens, 2016: Arctic observation and reanalysis integrated System: a new data product for validation and climate Study. *Bull. Amer. Meteor. Soc.*, **97**, 907-916.
- Day, J. J., J. C. Hargreaves, J. D. Annan, and A. Abe-Ouchi, 2012: Sources of multi-decadal variability in Arctic se ice extent. *Environ. Res. Lett.*, 7, 03011.
- Deser, C., and H. Teng, 2008: Evolution of Arctic sea ice concentration trends and the role of atmospheric circulation forcing, 1979–2007. *Geophys. Res. Lett.*, **35**, L02504.
- Deser, C., and Coauthors, 2020: Insights from earth system model initial-condition large ensembles and future prospects. *Nat. Clim. Change*, **10**, 277–286.
- Ding, Q., J. M. Wallace, D. S. Battisti, E. J. Steig, A. J. E. Gallant, H. J. Ki, and L Geng, 2014: Tropical forcing of the recent rapid Arctic warming in northeastern Canada and Greenland. *Nature*, **509**, 209-212.
- Ding, Q., and Coauthors, 2017: Influence of the recent high-latitude atmospheric circulation change on summertime Arctic sea ice. *Nat. Clim. Chang.*, 7, 289–295.
- Ding, Q., and Coauthors, 2019: Fingerprints of internal drivers of Arctic sea ice loss in observations and model simulations. *Nat. Geosci.*, **12**, 28–33.
- Dong, Y., C. Proistosescu, K. C. Armour, and D. S. Battisti, 2019: Attributing historical and future evolution of radiative feedbacks to regional warming patterns using a Green's function approach: the preeminence of the Western Pacific. *J. Climate*, **32**, 5471-5491.

- Donohoe, A., E. Blanchard-Wrigglesworth., A. Schweiger, and P. Rasch, 2020: The effect of atmospheric transmissivity on model and observational estimates of the sea ice albedo feedback. *J. Climate*, **3**, 5743-5765.
- Dörr, J., M. Årthun, T. Eldevik, and E. Madonna, 2021: Mechanisms of regional winter sea-ice variability in a warming Arctic. *J. Climate*, AOP, 1–56.
- England, M., A. Jahn, and L. Polvani, 2019: Nonuniform contribution of internal variability to recent Arctic sea ice loss. *J. Climate*, **32**, 4039-4053.
- England, M. R., L. M. Polvani, and L. Sun, 2020: Robust Arctic warming caused by projected Antarctic sea ice loss. *Environ. Res. Lett.*, **15**, 104005.
- Feng, X., and Coauthors, 2021: A multidecadal-scale tropically-driven global teleconnection over the past millennium and its recent strengthening. *J. Climate*, **34**, 2549-2565.
- Francis, J. A., and B. Wu, 2020: Why has no new record-minimum Arctic sea-ice extent occurred since September 2012? *Environ. Res. Lett.*, **15**, 114034.
- Fyfe, J. C., V. Kharin, B. D. Santer, R. N. S. Cole, and N. P. Gillett, 2021: Significant impact of forcing uncertainty in a large ensemble of climate model simulations. *Proc. Nat. Acad. Sci.*, 118, 23.
- Hersbach, H, and Coauthors, 2020: The ERA5 global reanalysis. Q. J. R. Meteorol. Soc., 146, 1999–2049.
- Huang, B., and Coauthors, 2017: Extended reconstructed sea surface temperature, version 5 (ERSSTv5): Upgrades, validations, and intercomparisons. *J. Climate*, **30**, 8179-8205.
- Huang Y, Q. Ding, X. Dong, B. Xi, and I. Baxter, 2021: Summertime low clouds mediate the impact of the large-scale circulation on Arctic sea ice. *Commun. Earth Environ.*, 2, 38.
- IPCC, 2021: Climate Change 2021: The Physical Science Basis. Contribution of Working Group I to the Sixth Assessment Report of the Intergovernmental Panel on Climate Change [Masson-Delmotte, V., P. Zhai, A. Pirani, S.L. Connors, C. Péan, S. Berger, N. Caud, Y. Chen, L. Goldfarb, M.I. Gomis, M. Huang, K. Leitzell, E. Lonnoy, J.B.R. Matthews, T.K. Maycock, T. Waterfield, O. Yelekçi, R. Yu, and B. Zhou (eds.)]. Cambridge University Press. In Press.
- Jahn, A., J. E. Kay, M. M. Holland, and D. M. Hall, 2016: How predictable is the timing of a summer ice-free Arctic? *Geophys. Res. Lett.*, **43**, 9113–9120.
- Jahn, A, 2018: Reduced probability of ice-free summers for 1.5 °C compared to 2 °C warming. *Nat. Clim. Chang.*, **8**, 409–413.
- Kay, J. E., M. M. Holland, and A. Jahn, 2011: Inter-annual to multi-decadal Arctic sea ice extent trends in a warming world. *Geophys. Res. Lett.*, **38**, L15708.
- Kay, J. E., and coauthors, 2014: The Community Earth System Model (CESM) Large Ensemble Project: A community resource for studying climate change in the presence of internal climate variability. *Bull. Amer. Meteor. Soc.*, **96**, 1333-1349.

- Labe, Z., G. Magnusdottir, and H. Stern, 2018: Variability of Arctic sea ice thickness using PIOMAS and the CESM Large Ensemble. *J. Climate*, **31**, 3233-3247.
- Lehner, F., F. Joos, C. C. Raible, J. Mignot, A. Born, K. M. Keller, and T. F. Stocker, 2015: Climate and carbon cycle dynamics in a CESM simulation from 850 to 2100 CE. *Earth Sys. Dyn.*, **6**, 411-434.
- Jeong, H., H.-S. Park, M. F. Stuecker, and S.-W. Yeh, 2022: Distinct impacts of major El Niño events on Arctic temperatures due to differences in eastern tropical Pacific sea surface temperatures, *Sci. Adv.*, **8**, eabl8278.
- Li, D., R. Zhang, and T. R. Knutson, 2017: On the discrepancy between observed and CMIP5 multi-model simulated Barents Sea winter sea ice decline. *Nat. Commun.*, **8**, 14991.
- Li, Z., Q. Ding, M. Steele, A. Schweiger, 2022: Recent upper Arctic Ocean warming expedited by summertime atmospheric processes. *Nat. Commun.*, **13**, 362.
- Liang, X., X. Li, H. Bi, M. Losch, Y. Gao, F. Zhao, Z. Tian, and C. Liu, 2022: A comparison of factors that led to the extreme sea ice minima in the twenty-first century in the Arctic Ocean. *J. Climate*, **35**, 1249-1265.
- Light, B., S. Dickinson, D. K. Perovich, and M. M. Holland, 2014: Evolution of summer Arctic sea ice albedo in CCSM4 simulations: Episodic summer snowfall and frozen summers. *J. Geophys. Res. Oceans*, **120**, 284-303.
- Liu, J. P., M. Song, R. M. Horton, and Y. Hu, 2013: Reducing spread in climate model projections of a September ice-free Arctic. *Proc. Natl. Acad. Sci.*, **110**, 12571-12576.
- Loeb, N. G., and Coauthors, 2018: Clouds and the Earth's Radiant Energy System (CERES) Energy Balanced and Filled (EBAF) Top-of-Atmosphere (TOA) edition-4.0 data product. *J. Climate*, **31**, 895-918.
- Meehl, G. A., C. T. Y. Chung, J. M. Arblaster, M. M. Holland, and C. M. Bitz, 2018: Tropical decadal variability and the rate of Arctic sea ice decrease. *Geophys. Res. Lett.*, **45**, 11,326–11,333.
- Meier, W. N., F. Fetterer, M. Savoie, S. Mallory, R. Duerr, and J. Stroeve, 2017: NOAA/NSIDCclimate data record of passive microwave sea ice concentration, version 3. Boulder, Colorado USA. NSIDC: National Snow and Ice Data Center.
- McCrystall, M. R., J. S. Hosking, I. P. White, and A. C. Maycock, 2020: The impact of changes in tropical sea surface temperatures over 1979–2012 on Northern Hemisphere high-latitude climate. *J. Climate*, **33**, 5103-5121.
- Muilwijk, M., and Coauthors, 2019: Arctic Ocean response to Greenland sea wind anomalies in a suite of model simulations. *J. Geophys. Res.*, **124**, 6286–6322.
- Notz, D., and J. Stroeve, 2016: Observed Arctic sea-ice loss directly follows anthropogenic CO2 emission. *Science*, **354**, 747–750.

- Notz, D. and Community, S. I. M. I. P., 2020: Arctic sea ice in CMIP6. *Geophys. Res. Lett.*, 47, e2019GL086749.
- Olonscheck, D., T. Mauritsen, and D. Notz, 2019: Arctic sea-ice variability is primarily driven by atmospheric temperature fluctuations. *Nat. Geosci.*, **12**, 430–434.
- Roach, L. A., and E. Blanchard-Wrigglesworth, 2022: Observed winds crucial for September Arctic sea ice loss. *Geophys. Res. Lett.*, **49**, e2022GL097884.
- Papritz, L., 2020: Arctic lower-tropospheric warm and cold extremes: Horizontal and vertical transport, diabatic processes, and linkage to synoptic circulation features. *J. Climate*, **33**, 993-1016. Polyakov, I. V., and Coauthors, 2020: Weakening of cold halocline layer exposes sea ice to oceanicheat in the eastern Arctic Ocean. *J. Climate*, **33**, 8107-8123.
- Rosenblum, E., and I. Eisenman, 2016: Faster Arctic sea ice retreat in CMIP5 than in CMIP3 due to volcanoes. *J. Climate*, **29**, 9179–9188.
- Schweiger, A. J., M. Steele, J. Zhang, G. W. K. Moore, and L. L. Kristin, 2021: Accelerated sea ice loss in the Wandel Sea points to a change in the Arctic's Last Ice Area. *Commun. Earth Environ.* 2, 122.
- Screen, J. A., and C. Deser, 2019: Pacific Ocean variability influences the time of emergence of a seasonally ice-free Arctic Ocean. *Geophys. Res. Lett.*, **46**, 2222-2231.
- Screen, J. A., 2021: An ice-free Arctic: what could it mean for European weather? *Weather*, **76**, 327-328.
- Seager, R., M. Cane, N. Henderson, D. E. Lee, R. Abernathey, and H. Zhang, 2019: Strengthening tropical Pacific zonal sea surface temperature gradient consistent with rising greenhouse gases. *Nat. Clim. Chang*, **9**, 517–522.
- Serreze, M. C., and R. G. Barry, 2011: Processes and impacts of Arctic amplification: A research synthesis. *Glob. Planet. Change*, 77, 85-96.
- Sigmond, M., and J. Fyfe, 2016: Tropical Pacific impacts on cooling North American winters. *Nat. Clim. Chang.*, **6**, 970–974.
- Stroeve, J. C., V. Kattsov, A. Barrett, M. Serreze, T. Pavlova, M. Holland, and W. N. Meier, 2012: Trends in Arctic sea ice extent from CMIP5, CMIP3 and observations. *Geophys. Res. Lett.*, **39**, L16502.
- Swart, N., J. Fyfe, E. Hawkins, E. K. Jennifer, and J. Alexandra, 2015: Influence of internal variability on Arctic sea-ice trends. *Nat. Clim. Chang.*, **5**, 86–89.
- Taylor, K. E., R. J. Stouffer, G. A. Meehl, 2012: An overview of CMIP5 and the experiment design. *Bull. Am. Meteorol. Soc.*, **93**, 485–498.
- Topal, D., Q. Ding, J. Mitchell, I. Baxter, M. Herein, T. Haszpra, R. Luo, and Q Li, 2020: An internal atmospheric process determining summertime Arctic sea ice melting in the next three

- decedes: lessons learned from five large ensembles and multiple CMIP5 climate simulations. J. *Climate*, **33**, 7431-7454.
- Trenberth, K. E., J. T. Fasullo, G. Branstator, and A. S. Phillips 2014: Seasonal aspects of the recent pause in surface warming. *Nat. Clim. Chang.*, **4**, 911–916.
- Wang, M., and J. E. Overland, J. E., 2009: A sea ice free summer Arctic within 30 years? *Geophys. Res. Lett.*, **36**, L07502.
- Wang, Q., and Coauthors, 2019: Ocean heat transport into the Barents Sea: Distinct controls on the upward trend and interannual variability. *Geophys. Res. Lett.*, **46**, 13180–13190.
- Wengel, C., S. S. Lee, M. F. Stuecker, A. Timmermann, J. E. Chu, and F. Schloesser, 2021: Future high-resolution El Niño/Southern Oscillation dynamics. *Nat. Clim. Chang.*, **11**, 758–765.
- Winton, M, 2011: Do climate models underestimate the sensitivity of Northern Hemisphere sea ice cover? *J. Climate*, **24**, 3924–3934.
- Webster, M. and Coauthors, 2018: Snow in the changing sea-ice systems. *Nat. Clim. Chang.*, **8**, 946-953.
- Wernli, H., and L. Papritz, 2018: Role of polar anticyclones and mid-latitude cyclones for Arctic summertime sea-ice melting. *Nat. Geosci.*, **11**, 108-113.
- Yang, W., and Coauthors, 2019: Climate impacts from large volcanic eruptions in a high-resolution climate model: The importance of forcing structure. *Geophys. Res. Lett.*, **46**, 7690-7699.
- Yeager, S. G., A. R. Karspeck, and G. Danabasoglu, 2015: Predicted slowdown in the rate of Atlantic sea ice loss. *Geophys. Res. Lett.*, **42**, 10-704.
- Zhang, R, 2015: Mechanisms for low-frequency variability of summer Arctic sea ice extent. *Proc. Natl Acad. Sci.*, **112**, 4570–4575.
- Zschenderlein, P., A. H. Fink, S. Pfahl, and H. Wernli, 2019: Processes determining heat waves across different European climates. *Quart. J. Roy. Meteor. Soc.*, **145**, 2973–2989.